Quantum Interference between Quasi-2D Fermi Surface Sheets in UTe_2

T. I. Weinberger,[1,*] Z. Wu,[1,*] D. E. Graf,[2] Y. Skourski,[3] A. Cabala,[4] J. Pospíšil,[4] J. Prokleška,[4] T. Haidamak,[4] G. Bastien,[4] V. Sechovský,[4] G. G. Lonzarich,[1] M. Vališka,[4] F. M. Grosche,[1] and A. G. Eaton[1,†]

[1]*Cavendish Laboratory, University of Cambridge, JJ Thomson Avenue, Cambridge CB3 0HE, United Kingdom*

[2]*National High Magnetic Field Laboratory, Tallahassee, Florida 32310, USA*

[3]*Hochfeld-Magnetlabor Dresden (HLD-EMFL), Helmholtz-Zentrum Dresden-Rossendorf, Dresden 01328, Germany*

[4]*Charles University, Faculty of Mathematics and Physics, Department of Condensed Matter Physics, Ke Karlovu 5, Prague 2, 121 16 Czech Republic*

(Received 6 October 2023; revised 15 February 2024; accepted 22 May 2024; published 26 June 2024)

UTe_2 is a spin-triplet superconductor candidate for which high quality samples with long mean free paths have recently become available, enabling quantum oscillation measurements to probe its Fermi surface and effective carrier masses. It has recently been reported that UTe_2 possesses a 3D Fermi surface component [Phys. Rev. Lett. **131**, 036501 (2023)]. The distinction between 2D and 3D Fermi surface sections in triplet superconductors can have important implications regarding the topological properties of the superconductivity. Here we report the observation of oscillatory components in the magnetoconductance of UTe_2 at high magnetic fields. We find that these oscillations are well described by quantum interference between quasiparticles traversing semiclassical trajectories spanning magnetic breakdown networks. Our observations are consistent with a quasi-2D model of this material's Fermi surface based on prior dHvA-effect measurements. Our results strongly indicate that UTe_2—which exhibits a multitude of complex physical phenomena—possesses a remarkably simple Fermi surface consisting exclusively of two quasi-2D cylindrical sections.

DOI: 10.1103/PhysRevLett.132.266503

Young's double slit experiment represents a powerful example of the wave-particle duality of photons [1]. A century later Davisson and Germer observed a similar phenomenon involving the quantum mechanical interference of a beam of electrons incident on a crystalline target [2,3]. In the solid state, superconducting quantum interference devices provide exceptionally accurate measurements of magnetic flux via diffraction-modulated interferometry [4,5]. For the case of normal metals, the manifestation of quantum interference (QI) effects in the magnetoconductance was first predicted by Shiba and Fukuyama [6], and soon thereafter experimentally realized by Stark and Friedberg in their measurements of the magnetoresistance of magnesium [7]. The concept of the Stark interferometer is based on interference between semiclassical quasiparticle trajectories across magnetic breakdown networks connecting separate Fermi surface (FS) sections, yielding oscillations in the conductivity that are periodic in inverse magnetic field strength [8–11].

Since the seminal experiments by Stark and co-workers, quantum interference oscillations (QIOs) have been observed in a variety of materials [12–16] including, in particular, a number of organic metals with quasi-2D (Q2D) FSs [17–24]. Unlike quantum oscillations (QOs) from the de Haas-van Alphen (dHvA) or Shubnikov-de Haas (SdH) effects, in which phase coherence and Landau quantization of quasiparticles traversing orbits corresponding to closed FS sections provide a direct measurement of the FS [11], QIOs only yield an indirect probe of the FS, as their frequencies correspond to k-space orbits spanning separate FS sections. Therefore, QIOs are only observed in materials in which the k-space separation of FS sections is sufficiently small for quasiparticles to tunnel between FS sheets in accessible magnetic field strengths [11,25]. It is important to note that QI is exclusively a kinetic effect and is thus observable in the electrical transport—unlike the dHvA effect, QIOs do not correspond to an oscillatory component of the free energy, therefore QI effects *cannot* be observed in bulk thermodynamic properties such as the magnetization [9,10,17,26].

Here, we report the observation of QIOs at high magnetic fields in contactless resistivity measurements of the heavy fermion paramagnetic metal UTe_2. This material has recently shown promising signs of being a spin-triplet superconductor [27–29], similar to the analogous

ferromagnetic compounds UGe_2, URhGe, and UCoGe [30–32]. Evidence indicating triplet pairing in UTe_2 comes from a number of sources including small changes in the NMR Knight shift on cooling through the superconducting critical temperature T_c [29,33] along with anisotropic upper critical fields that far exceed the Pauli limit for singlet pairing [27,34–36]. Recent advances in the growth procedure of single crystal UTe_2 specimens have led to a marked enhancement in crystalline quality, enabling the observation of QOs from the dHvA effect [37,38]. The angular profile of the dHvA data is indicative of a relatively simple Q2D FS, consisting of one electron-type and one hole-type cylinder, each hosting quasiparticles of heavy effective masses $\sim 40\ m_e$ [37,38].

Methods.—UTe_2 single crystals were grown by a molten salt flux technique [39] using the methodology detailed in Ref. [38]. This technique has been shown to yield high quality specimens of $T_c \approx 2.1$ K with long mean free paths of the order of 100 nm [36–39]. Details regarding sample characterization are given in the Supplemental Material [40]. Contactless resistivity measurements were performed in static fields to 41.5 T at the National High Magnetic Field Lab, Tallahassee, Florida, using the tunnel diode oscillator (TDO) technique [52]; similar measurements were obtained in pulsed fields to 70 T at the Hochfeld-Magnetlabor, HZDR, Dresden, using the proximity detector oscillator (PDO) technique [53,54].

Results.—Figure 1 shows the background-subtracted TDO signal (Δf_{TDO}) for magnetic field oriented 8° away from the crystalline c axis towards the a axis ($\theta_c = 8°$) [55]. The fast Fourier transform (FFT) of the Δf_{TDO} data reveals four clear frequency branches, which we label as α–δ. Notably, the FFT spectra at $\theta_c = 8°$ of the TDO signal are very different from the spectra we observed in our prior dHvA study at the same angle (Ref. [38]), implying that these are not QOs stemming from the SdH effect. Furthermore, the amplitude of dHvA QOs diminished by almost an order of magnitude between 19 mK and 200 mK —whereas here the signal is large and very well resolved at 400 mK. These observations indicate that the oscillations in f_{TDO} are likely QIOs not QOs, as QIOs generally correspond to reciprocal space areas constructed from sums and differences between FS sections, and often exhibit effective masses much lower than those of dHvA and SdH QOs [13,17,18].

Using our FS model from Ref. [38], we illustrate in Figs. 1 and 2 how the frequencies of the α–δ FFT peaks correspond remarkably well to k-space areas *between* the cylindrical Fermi sheets, which are centered at the center and corners of the first Brillouin zone (BZ). Each of these frequency components can thus be well understood as coming from QI between two quasiparticles—one making two orbits around a FS cylinder, and the other traversing a magnetic breakdown (MB) network between two cylinders of the same carrier type.

To show this, we consider the generalized theory of MB orbits given by Kaganov and Slutskin [26]. In a magnetic field B the oscillatory component of a kinetic coefficient,

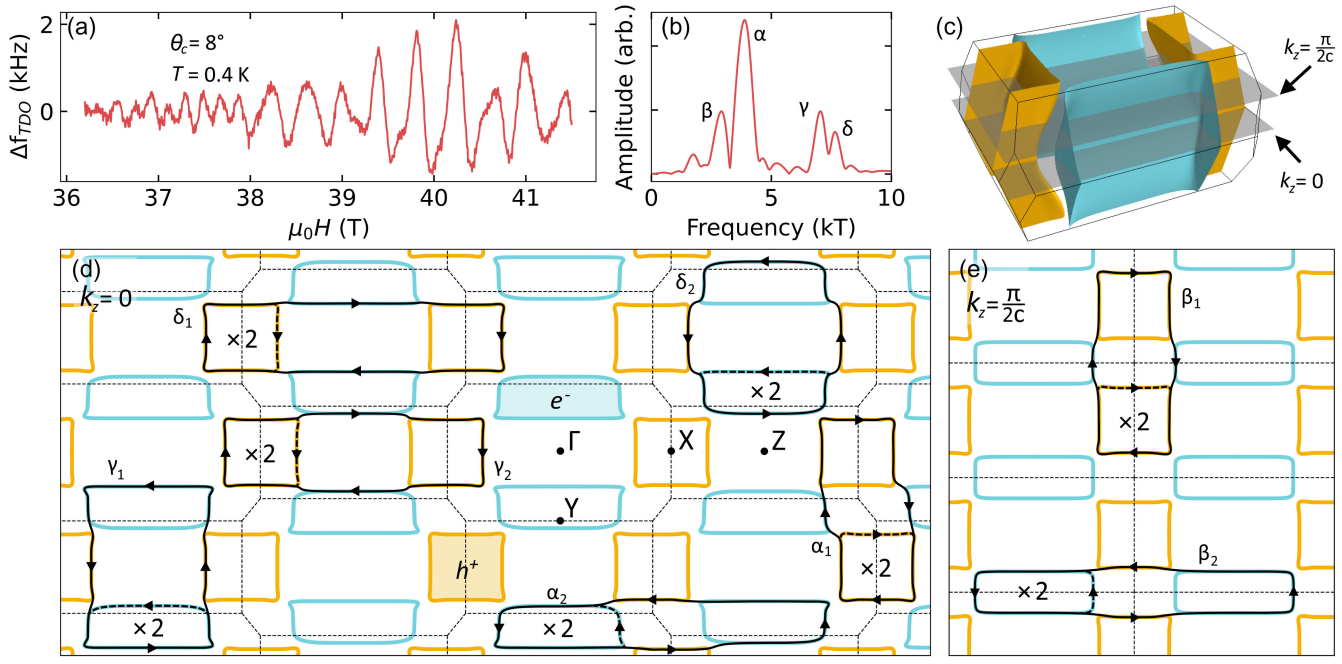

FIG. 1. (a) QIOs in the contactless resistivity of UTe_2 and (b) the corresponding FFT spectra. (c) Our Fermi surface model for UTe_2 adapted from Ref. [38], with the planes $k_z = 0$ and $k_z = (\pi/2c)$ indicated. (d) An extended-zone view, with the c axis into the page, at $k_z = 0$ and (e) at $k_z = (\pi/2c)$. QI trajectories enclosing areas that correspond to the QIO frequencies α–δ are indicated; note that each enclosed area α–δ has two distinct MB networks corresponding to it (denoted as $\lambda_{1,2}$).

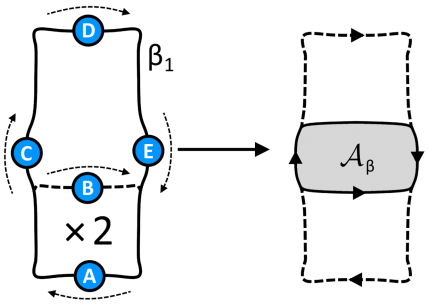

FIG. 2. Schematic of two semiclassical quasiparticle trajectories that interfere to give the f_β frequency component. The difference in area of the paths *ACDEA* and *ABABA* is equal to $\mathcal{A}_\beta$, as shown in the text. Note that the orbit *CDEBC* is not possible due to the direction of the Lorentz force (indicated with arrows). The frequency components α, γ, and δ come from QI between analogous networks, as traced out in Fig. 1.

such as the electrical conductivity, is composed of harmonics of the form

$$\sum_{\lambda,\lambda'} \exp[i(\phi_\lambda - \phi_{\lambda'})] = \sum_{\lambda,\lambda'} \exp\left(\frac{i\hbar}{eB}\mathcal{A}_{\lambda,\lambda'}\right) \qquad (1)$$

for phase ϕ where λ and λ' are the two semiclassical quasiparticle paths that share a common start and end point, enclosing between them an area in reciprocal space of $\mathcal{A}_{\lambda,\lambda'}$ [18,56].

Take for example the area $\mathcal{A}_\beta$ shaded in Fig. 2, which sits at the corner of the first BZ for $k_z = (\pi/2c)$. Writing the area of the hole-type FS cylinder as $\mathcal{A}_{h^+}$, we can see that the area $\mathcal{A}_\beta$ is equal to the difference of the areas enclosed by the paths $\lambda = ACDEA$ and $\lambda' = ABABA$ as $\mathcal{A}_{ACDEA} - \mathcal{A}_{ABABA} = (2\mathcal{A}_{h^+} + \mathcal{A}_\beta) - 2\mathcal{A}_{h^+} = \mathcal{A}_\beta$. Similarly, areas corresponding to the α, γ, and δ frequency components are formed by QI between the quasiparticle trajectories traced in Fig. 1 [57]. The probability of a quasiparticle traversing a path depends on the number of MB tunneling events (each of probability amplitude p) and Bragg reflections (of probability amplitude q) that are contained within the path, where $|p|^2 = P = \exp(-B_0/B)$ for breakdown field B_0 and $q = i\sqrt{(1-P)}$ [11,17,18,25,58]. Therefore, the probability amplitudes for quasiparticles to traverse the paths $\lambda = ACDEA$ and $\lambda' = ABABA$, corresponding to the β frequency in Fig. 2, are $q^4p^4\exp(i\phi_\lambda)$ and $q^8\exp(i\phi_{\lambda'})$, respectively. Because of this exponentially suppressed tunneling probability—which necessitates the application of high magnetic fields—we limit our discussion just to the lowest order relevant networks as depicted in Fig. 1, each of which requires only four instances of MB.

By Eq. (1), the probability of quasiparticles traversing the paths in Fig. 2 will involve oscillating terms including some proportional to $\cos[\phi_\lambda - \phi_{\lambda'}] = \cos[2\pi(2f_{h^+} + f_\beta - 2f_{h^+})/B] = \cos[2\pi f_\beta/B]$, which will contribute to the (real part of the) conductivity. Furthermore, in the low temperature limit the temperature dependence of QIOs simply follows the Lifshitz-Kosevich theory [11,13,59] with an apparent effective mass $m^*_{\lambda,\lambda'}$, which is proportional to the dependence of the phase on the electron energy, E_k:

$$m^*_{\lambda,\lambda'} = \frac{e\hbar B}{2\pi}\left|\frac{\partial(\phi_\lambda - \phi_{\lambda'})}{\partial E_k}\right| = |m^*_\lambda - m^*_{\lambda'}| \qquad (2)$$

where m^*_λ ($m^*_{\lambda'}$) denotes the effective mass of path λ (λ') [13,18]. Note that it is the *difference* in the effective masses of the two interfering paths that determines the apparent effective mass of QIOs—thus enabling QIOs to be observed to much higher temperatures than QOs from the dHvA and SdH effects [13,17–19].

Figure 3 shows that the γ and δ frequencies in the QIO spectra of UTe_2 exhibit apparent effective masses ($\approx 5\ m_e$) almost an order of magnitude lower than the quasiparticle effective masses reported for dHvA QOs ($\sim 40\ m_e$) [37,38], showing that the subtraction of masses between the two trajectories in Eq. (2) has almost canceled out. By contrast, the α and β frequencies are much heavier with masses in the region of 20–35 m_e (Fig. 3 and Fig. S3 in the Supplemental Material). This implies that these MB networks span FS sections with a highly anisotropic distribution of the Fermi velocity, v_F. This is consistent with several experimental [37,38,60] and theoretical [61,62] studies that indicate the hybridization between U f electrons with the U d bands and Te p bands, which provides the dominant contribution to the Q2D FS, can result in significant variations in the effective quasiparticle masses at points around the cylindrical sheets. We note that our uncertainty in m^*_α and m^*_β is considerably larger than for m^*_γ and m^*_δ due to these frequencies only being observable near the base temperature of the ^{3}He cryostat used for this measurement, with the uncertainty in temperature dominating the uncertainty in $m^*_{\alpha,\beta}$. Further measurements in the experimentally challenging temperature-field regime of ≤ 200 mK and ≥ 40 T are required to carefully probe the anisotropy of v_F around the FS of UTe_2, and thus to better understand the hybridization of the f, d, and p bands.

In principle, an infinite number of MB networks could give rise to QIOs. Thus, it is expected that orbits of the type $\mathcal{A}_{ACDEA} - \mathcal{A}_{ABA} = (2\mathcal{A}_{h^+} + \mathcal{A}_\beta) - \mathcal{A}_{h^+} = \mathcal{A}_\beta + \mathcal{A}_{h^+}$ should occur. However, the effective mass associated with these orbits would be greater than the masses of the hole and electron orbits from which they arise. If in the most simple case we assume that the breakdown orbits of type $\mathcal{A}_{ACDEA}$ have masses of $2m^*_{h^+/e^-} + \epsilon_m$, where ϵ_m is a small difference to account for the fact that quasiparticles are in fact not traversing full FS sheets, then by Eq. (2) these breakdown orbits need to interfere with two full FS sheet orbits to produce oscillations of $m^* = \epsilon_m$. By comparison, orbits of the type $\mathcal{A}_{ACDEA} - \mathcal{A}_{ABA}$ would instead have

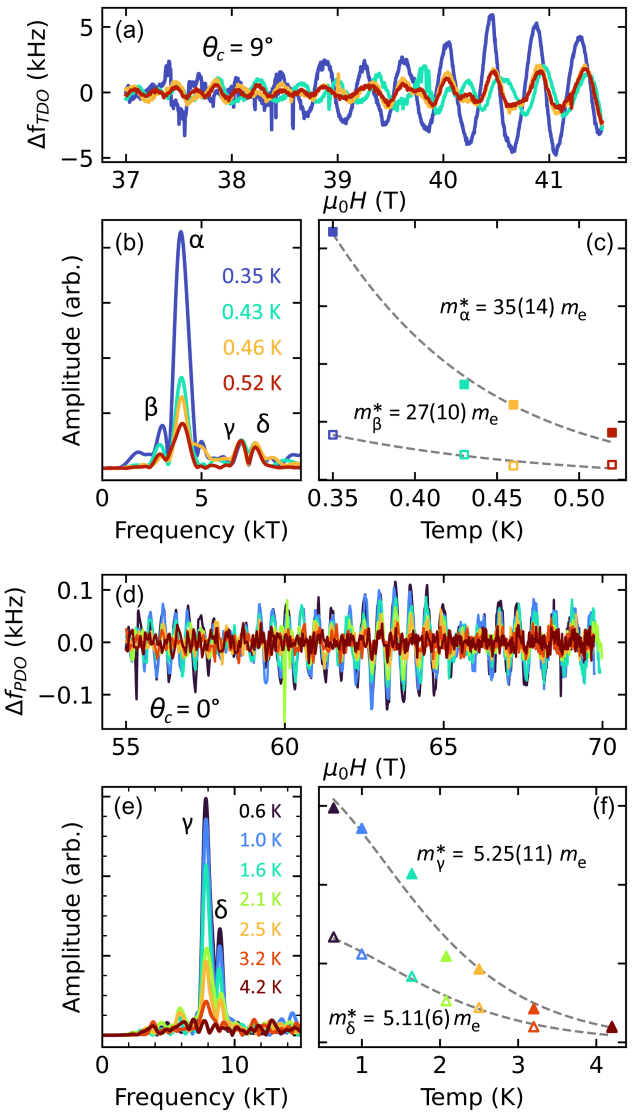

FIG. 3. QIOs, FFTs, and apparent effective masses for (a)–(c) steady field measurements focussing on the α and β frequency components, and (d)–(f) higher temperature pulsed field measurements focussing on the γ and δ components. The effective masses m^*_γ and m^*_δ are markedly lower than those observed in dHvA-effect measurements for the same field orientation [38].

masses of $m^* = m^*_{h^+/e^-} + \epsilon_m$ and as such would be too heavy to observe at ^{3}He temperatures.

Figure 4 shows the evolution of the QIO frequency with a magnetic field tilt angle, and compares with the prediction from our Q2D FS model [in panel (c)]. Although this is only a crude approximation of the expected QIO frequency profile, we find remarkably good agreement between our FS model adapted from Ref. [38] and the QIOs we observe in TDO measurements. This result gives strong confidence that the FS of UTe_2 is very well described by our Q2D model.

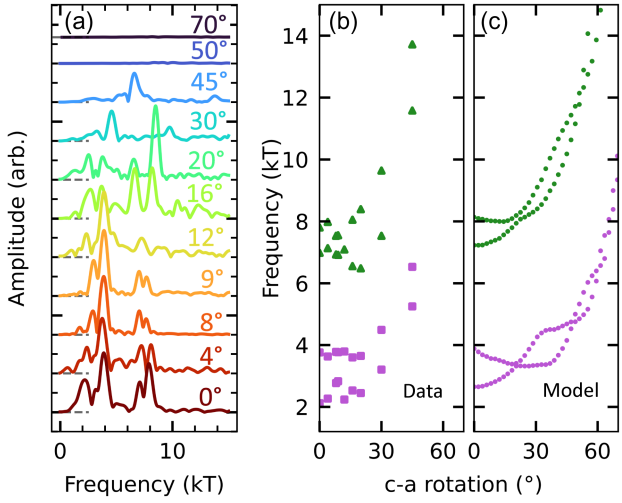

FIG. 4. (a) Evolution of FFT spectra as a function of magnetic field tilt angle away from the c axis. (b) Frequency versus angle for the α and β branches (in purple) and the γ and δ branches (in green). (c) The expectation of the angular frequency profile corresponding to the areas $\mathcal{A}_{\alpha,\beta,\gamma,\delta}$ computed from our FS model depicted in Fig. 1. Surprisingly good correspondence between model prediction and experimental measurement is observed, given the simplicity of the model assumptions (given in the Supplemental Material).

Our discussion so far has focussed on field aligned coaxially to the FS cylinders (along c), and at inclination angles close to c. Figure 5 shows that for field oriented along the a axis, two additional frequencies $f_\zeta = 220$ T and $f_\eta = 4.5$ kT are observed. Again, the enclosed areas of these MB networks correspond very well to our Q2D FS model [Fig. 5(f)]. The low frequency ζ oscillations for field along a are of considerable amplitude and are clearly observable in the raw TDO signal without background subtraction [Fig. 5(a)]. Along the a axis, ζ again corresponds to a QIO, whereas η is consistent with a conventional MB orbit, which may explain its small amplitude as well as its observation for B only directly along the a axis.

We note that a similar study of oscillations in the TDO signal of UTe_2 at high fields was recently reported [63]. For $B \| a$ Ref. [63] reports an oscillatory frequency of 223 T, in very good agreement with the 220 T ζ orbit we observe at this field orientation (Fig. 5). However, rather than being of a QI origin, the authors of Ref. [63] interpreted the observed oscillatory waveform to comprise QOs from the SdH-effect caused by the presence of a light 3D FS pocket(s). The distinction between Q2D and 3D FS dimensionality in the case of UTe_2 is important, as any 3D pockets could have significant implications regarding the topological properties of the putatively spin-triplet superconductivity [64,65].

However, in our measurements we do not observe any indication of the presence of a 3D FS pocket. Figure 5(b) shows the evolution of Δf_{TDO} as the field is tilted away

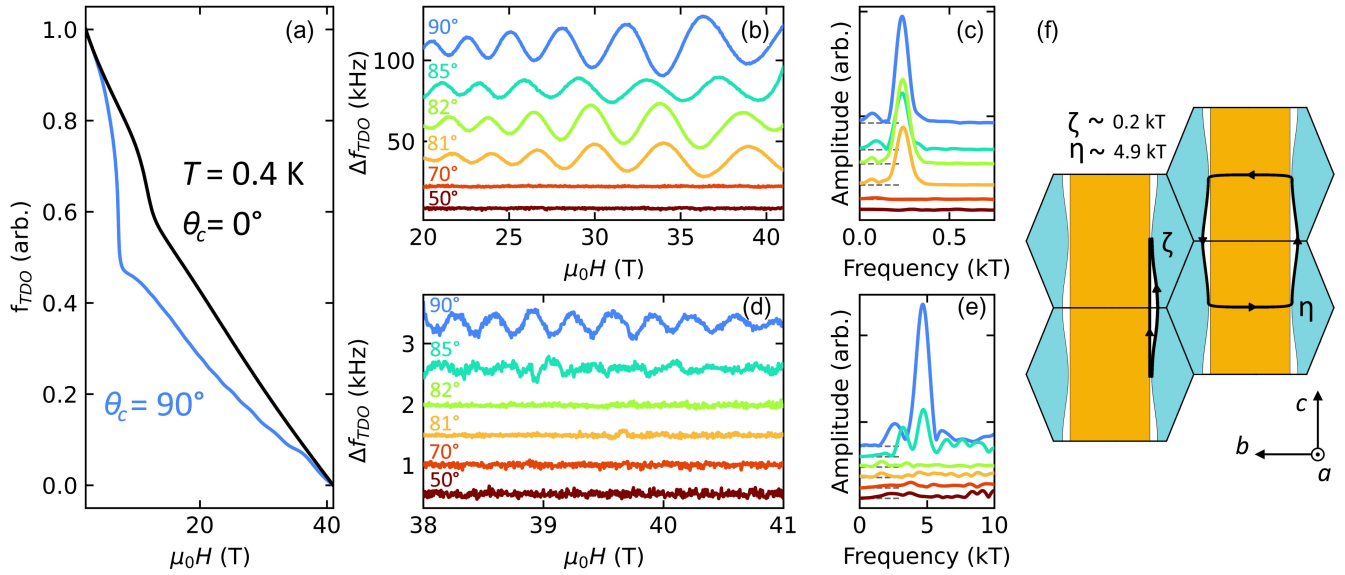

FIG. 5. (a) Raw TDO signal for magnetic field oriented along the c axis ($\theta_c = 0°$) and along the a axis ($\theta_c = 90°$). (b) QIOs at θ_c angles as indicated over 20–41.5 T and (c) their corresponding FFTs. (d) High frequency oscillations at $\theta_c = 90°$ are quickly suppressed by rotation away from the a axis. (e) FFTs of the curves in panel (d). Only the data at $\theta_c = 90°$ has a resolvable frequency component above the noise floor of the measurement. (f) A side view of the cylindrical sheets of our Q2D FS model (compared to the axial view given in Fig. 1). The trajectories ζ and η are identified, which enclose areas with very good correspondence to the oscillatory frequencies observed for magnetic field orientated along the a axis.

from a towards c. For magnetic field oriented along the a axis we observe low frequency large amplitude oscillations, in good agreement with the raw data presented in Ref. [63]. A large oscillatory component is still visible 9° away from a; however, after a rotation of 20° (to $\theta_c = 70°$) no oscillations are observed within the resolution of the measurement. This is inconsistent with this frequency branch coming from SdH-effect QOs due to a 3D pocket; however, this behavior is consistent with a QI interpretation of the oscillatory origin, as the ζ trajectory is only possible for B close to a. In the Supplemental Material we show a similar evolution for rotating away from a towards b. Furthermore, no slow oscillations at these tilt angles have been reported in prior dHvA measurements by the field modulation [37] or torque magnetometry [38] techniques—they appear only to be observed in the electrical conductivity, again consistent with a QI origin.

The stark difference in the effective masses of the α, β and γ, δ components implies a strong anisotropy of $v_F(\mathbf{k})$. In our recent study of dHvA QOs in UTe_2 we observed twofold effective mass variations along the measured frequency branches under rotation away from the c axis [38]. In order to attain such a variation, this implies a significant anisotropy of $v_F(k_z)$, which in turn could account for the large difference in effective masses of the QIOs. Such a variation in effective mass likely stems from substantial hybridization between U d bands and Te p bands, which are the main contributors to the Q2D FS sheets [62], and an f-electron band sitting just above the Fermi level. This band has been detected in ARPES measurements, in which a significant spectral weight was observed at the Z point of the BZ [60]. Models of UTe_2 that include the presence of such a band [61,62] show that the effect of the U f electrons hybridizing with U d bands is to compress them in energy, effectively increasing their band mass [66]. It is therefore likely that v_F is lowest (and thus m^* is highest) at the regions of the FS cylinders that are closest to the Z point, as here the spectral contribution of the f electrons is largest and thus the hybridization with them will be the greatest.

In summary, we measured the contactless resistivity of UTe_2 to high applied magnetic field strengths. We observed oscillatory components that are well explained by quantum interference between semiclassical quasiparticle trajectories spanning magnetic breakdown networks. We find that the quantum interference frequencies correspond very well to a quasi-2D model of the UTe_2 Fermi surface. Our observations give no indication of the presence of any 3D Fermi surface pockets in this material.

We are grateful to N. R. Cooper, D. V. Chichinadze, D. Shaffer, A. J. Hickey, H. Liu, P. Coleman, J. Chen, C. K. de Podesta, O. P. Squire, T. Helm, and especially A. F. Bangura for stimulating discussions. We thank T. J. Brumm and S. T. Hannahs for technical advice and assistance. This project was supported by the EPSRC of the UK (Grants No. EP/X011992/1 and No. EP/R513180/1). A portion of this work was performed at the National High Magnetic Field Laboratory, which is supported by National Science Foundation Cooperative Agreement No. DMR-2128556

and the State of Florida. We acknowledge support of the HLD at HZDR, a member of the European Magnetic Field Laboratory (EMFL). The EMFL also supported dual access to facilities at MGML, Charles University, Prague, under the European Union's Horizon 2020 research and innovation programme through the ISABEL project (No. 871106). Crystal growth and characterization were performed at MGML [67], which is supported within the program of Czech Research Infrastructures (Project No. LM2023065). We acknowledge financial support by the Czech Science Foundation (GACR), Project No. 22-22322S. T. I. W. and A. G. E. acknowledge support from QuantEmX grants from ICAM and the Gordon and Betty Moore Foundation through Grants No. GBMF5305 and No. GBMF9616. A. G. E. acknowledges support from the Henry Royce Institute for Advanced Materials through the Equipment Access Scheme enabling access to the Advanced Materials Characterisation Suite at Cambridge, Grants No. EP/P024947/1, No. EP/M000524/1, and No. EP/R00661X/1; and from Sidney Sussex College (University of Cambridge).

*These authors contributed equally to this work.
†alex.eaton@phy.cam.ac.uk

[1] T. Young, I. The Bakerian Lecture. Experiments and calculations relative to physical optics, Phil. Trans. R. Soc. London **94**, 1 (1804).
[2] C. Davisson and L. H. Germer, The scattering of electrons by a single crystal of nickel, Nature (London) **119**, 558 (1927).
[3] C. Davisson and L. H. Germer, Diffraction of electrons by a crystal of nickel, Phys. Rev. **30**, 705 (1927).
[4] B. D. Josephson, Possible new effects in superconductive tunnelling, Phys. Lett. **1**, 251 (1962).
[5] J. E. Mercereau, *Superconductivity*, edited by R. D. Parks (Marcel Dekker, New York, 1969), Vol. 1.
[6] H. Shiba and H. Fukuyama, A quantum theory of galvanomagnetic effect in metals with magnetic breakdown. I, J. Phys. Soc. Jpn. **26**, 910 (1969).
[7] R. Stark and C. Friedberg, Quantum interference of electron waves in a normal metal, Phys. Rev. Lett. **26**, 556 (1971).
[8] R. Stark and C. Friedberg, Interfering electron quantum states in ultrapure magnesium, J. Low Temp. Phys. **14**, 111 (1974).
[9] R. Stark and R. Reifenberger, Quantitative theory for the quantum interference effect in the transverse magnetoresistance of pure magnesium, J. Low Temp. Phys. **26**, 763 (1977).
[10] D. Morrison and R. Stark, Two-lifetime model calculations of the quantum interference dominated transverse magnetoresistance of magnesium, J. Low Temp. Phys. **45**, 531 (1981).
[11] D. Shoenberg, *Magnetic Oscillations in Metals* (Cambridge University Press, Cambridge, England, 1984), 10.1017/CBO9780511897870.
[12] S. Uji, T. Terashima, H. Aoki, J. S. Brooks, M. Tokumoto, S. Takasaki, J. Yamada, and H. Anzai, Rapid oscillations in the organic conductor $(TMTSF)_2ClO_4$, Phys. Rev. B **53**, 14399 (1996).
[13] N. Harrison, R. G. Goodrich, J. J. Vuillemin, Z. Fisk, and D. G. Rickel, Quantum interference in LaB_6, Phys. Rev. Lett. **80**, 4498 (1998).
[14] N. Harrison, D. W. Hall, R. G. Goodrich, J. J. Vuillemin, and Z. Fisk, Quantum interference in the spin-polarized heavy fermion compound CeB_6: Evidence for topological deformation of the Fermi surface in strong magnetic fields, Phys. Rev. Lett. **81**, 870 (1998).
[15] D. Graf, J. S. Brooks, E. S. Choi, M. Almeida, R. T. Henriques, J. C. Dias, and S. Uji, Quantum interference in the quasi-one-dimensional organic conductor $(Per)_2Au(mnt)_2$, Phys. Rev. B **75**, 245101 (2007).
[16] N. L. Nair, M.-E. Boulanger, F. Laliberté, S. Griffin, S. Channa, A. Legros, W. Tabis, C. Proust, J. Neaton, L. Taillefer, and J. G. Analytis, Signatures of possible surface states in TaAs, Phys. Rev. B **102**, 075402 (2020).
[17] N. Harrison, J. Caulfield, J. Singleton, P. Reinders, F. Herlach, W. Hayes, M. Kurmoo, and P. Day, Magnetic breakdown and quantum interference in the quasi-two-dimensional superconductor κ-$(BEDT\text{-}TTF)_2Cu(NCS)_2$ in high magnetic fields, J. Phys. Condens. Matter **8**, 5415 (1996).
[18] M. V. Kartsovnik, G. Y. Logvenov, T. Ishiguro, W. Biberacher, H. Anzai, and N. D. Kushch, Direct observation of the magnetic-breakdown induced quantum interference in the quasi-two-dimensional organic metal κ-$(BEDT\text{-}TTF)_2CU(NCS)_2$, Phys. Rev. Lett. **77**, 2530 (1996).
[19] J. Singleton, Studies of quasi-two-dimensional organic conductors based on BEDT-TTF using high magnetic fields, Rep. Prog. Phys. **63**, 1111 (2000).
[20] J. M. Schrama, J. Singleton, R. S. Edwards, A. Ardavan, E. Rzepniewski, R. Harris, P. Goy, M. Gross, J. Schlueter, M. Kurmoo *et al.*, Millimetre-wave measurements of the bulk magnetoconductivity of anisotropic metals: application to the organic superconductors κ-$(BEDT\text{-}TTF)_2Cu(NCS)_2$ and β"-$(BEDT\text{-}TTF)_2SF_5CH_2CF_2SO_3$ (BEDT-TTF ≡ bis(ethylene-dithio)tetrathiafulvalene), J. Phys. Condens. Matter **13**, 2235 (2001).
[21] C. Proust, A. Audouard, L. Brossard, S. Pesotskii, R. Lyubovskii, and R. Lyubovskaya, Competing types of quantum oscillations in the two-dimensional organic conductor $(BEDT\text{-}TTF)_8Hg_4Cl_{12}(C_6H_5Cl)_2$, Phys. Rev. B **65**, 155106 (2002).
[22] M. V. Kartsovnik, High magnetic fields: A tool for studying electronic properties of layered organic metals, Chem. Rev. **104**, 5737 (2004).
[23] A. Audouard, D. Vignolles, C. Proust, L. Brossard, M. Nardone, E. Haanappel, S. Pesotskii, R. Lyubovskii, and R. Lyubovskaya, Magnetic oscillations in a two-dimensional network of coupled orbits, Physica (Amsterdam) **346B**, 377 (2004).
[24] R. Lyubovskii, S. Pesotskii, E. Zhilyaeva, A. Flakina, and R. Lyubovskaya, The electron structure of metallic layers in the quasi-two-dimensional dual-layered organic metal $(BETS)_4HgBr_4(C_6H_4Cl_2)$, Tech. Phys. Lett. **45**, 407 (2019).
[25] R. G. Chambers, Magnetic breakdown in real metals, Proc. Phys. Soc. **88**, 701 (1966).
[26] M. I. Kaganov and A. A. Slutskin, Coherent magnetic breakdown, Phys. Rep. **98**, 189 (1983).

[27] S. Ran, C. Eckberg, Q. P. Ding, Y. Furukawa, T. Metz, S. R. Saha, I. L. Liu, M. Zic, H. Kim, J. Paglione, and N. P. Butch, Nearly ferromagnetic spin-triplet superconductivity, Science **365**, 684 (2019).

[28] S. Ran, I. L. Liu, Y. S. Eo, D. J. Campbell, P. M. Neves, W. T. Fuhrman, S. R. Saha, C. Eckberg, H. Kim, D. Graf, F. Balakirev, J. Singleton, J. Paglione, and N. P. Butch, Extreme magnetic field-boosted superconductivity, Nat. Phys. **15**, 1250 (2019).

[29] D. Aoki, J. P. Brison, J. Flouquet, K. Ishida, G. Knebel, Y. Tokunaga, and Y. Yanase, Unconventional superconductivity in UTe_2, J. Phys. Condens. Matter **34**, 243002 (2022).

[30] S. S. Saxena, P. Agarwal, K. Ahilan, F. M. Grosche, R. K. W Haselwimmer, M. J. Steiner, E. Pugh, I. R. Walker, S. R. Julian, P. Monthoux, G. G. Lonzarich, A. Huxley, I. Sheikin, D. Braithwaite, and J. Flouquet, Superconductivity on the border of itinerant-electron ferromagnetism in UGe_2, Nature (London) **406**, 587 (2000).

[31] D. Aoki, A. Huxley, E. Ressouche, D. Braithwaite, J. Flouquet, J. P. Brison, E. Lhotel, and C. Paulsen, Coexistence of superconductivity and ferromagnetism in URhGe, Nature (London) **413**, 613 (2001).

[32] N. T. Huy, A. Gasparini, D. E. de Nijs, Y. Huang, J. C. P. Klaasse, T. Gortenmulder, A. de Visser, A. Hamann, T. Görlach, and H. v. Löhneysen, Superconductivity on the border of weak itinerant ferromagnetism in UCoGe, Phys. Rev. Lett. **99**, 067006 (2007).

[33] H. Matsumura, H. Fujibayashi, K. Kinjo, S. Kitagawa, K. Ishida, Y. Tokunaga, H. Sakai, S. Kambe, A. Nakamura, Y. Shimizu *et al.*, Large reduction in the a-axis knight shift on UTe_2 with $T_c = 2.1$ K, J. Phys. Soc. Jpn. **92**, 063701 (2023).

[34] B. Chandrasekhar, A note on the maximum critical field of high-field superconductors, Appl. Phys. Lett. **1**, 7 (1962).

[35] A. M. Clogston, Upper limit for the critical field in hard superconductors, Phys. Rev. Lett. **9**, 266 (1962).

[36] Z. Wu, T. I. Weinberger, J. Chen, A. Cabala, D. V. Chichinadze, D. Shaffer, J. Pospisil, J. Prokleska, T. Haidamak, G. Bastien, V. Sechovsky, A. J. Hickey, M. J. Mancera-Ugarte, S. Benjamin, D. E. Graf, Y. Skourski, G. G. Lonzarich, M. Valiska, F. M. Grosche, and A. G. Eaton, Enhanced triplet superconductivity in next generation ultraclean UTe_2, arXiv:2305.19033.

[37] D. Aoki, H. Sakai, P. Opletal, Y. Tokiwa, J. Ishizuka, Y. Yanase, H. Harima, A. Nakamura, D. Li, Y. Homma, Y. Shimizu, G. Knebel, J. Flouquet, and Y. Haga, First observation of the de Haas–van Alphen effect and Fermi surfaces in the unconventional superconductor UTe_2, J. Phys. Soc. Jpn. **91**, 083704 (2022).

[38] A. G. Eaton, T. I. Weinberger, N. J. M. Popiel, Z. Wu, A. J. Hickey, A. Cabala, J. Pospíšil, J. Prokleška, T. Haidamak, G. Bastien, P. Opletal, H. Sakai, Y. Haga, R. Nowell, S. M. Benjamin, V. Sechovský, G. G. Lonzarich, F. M. Grosche, and M. Vališka, Quasi-2D Fermi surface in the anomalous superconductor UTe_2, Nat. Commun. **15**, 223 (2024).

[39] H. Sakai, P. Opletal, Y. Tokiwa, E. Yamamoto, Y. Tokunaga, S. Kambe, and Y. Haga, Single crystal growth of superconducting UTe_2 by molten salt flux method, Phys. Rev. Mater. **6**, 073401 (2022).

[40] See Supplemental Material at http://link.aps.org/supplemental/10.1103/PhysRevLett.132.266503 for additional data and discussion, which includes Refs. [41–51].

[41] K. Semeniuk, H. Chang, J. Baglo, S. Friedemann, S. W. Tozer, W. A. Coniglio, M. B. Gamża, P. Reiss, P. Alireza, I. Leermakers *et al.*, Truncated mass divergence in a Mott metal, Proc. Natl. Acad. Sci. U.S.A. **120**, e2301456120 (2023).

[42] B. Ramshaw, S. Sebastian, R. McDonald, J. Day, B. Tan, Z. Zhu, J. Betts, R. Liang, D. Bonn, W. Hardy *et al.*, Quasiparticle mass enhancement approaching optimal doping in a high-T_c superconductor, Science **348**, 317 (2015).

[43] H. Liu, A. Hickey, M. Hartstein, A. Davies, A. Eaton, T. Elvin, E. Polyakov, T. Vu, V. Wichitwechkarn, T. Förster *et al.*, f-electron hybridised Fermi surface in magnetic field-induced metallic YbB_{12}, npj Quantum Mater. **7**, 12 (2022).

[44] P. F. S. Rosa, A. Weiland, S. S. Fender, B. L. Scott, F. Ronning, J. D. Thompson, E. D. Bauer, and S. M. Thomas, Single thermodynamic transition at 2 K in superconducting UTe_2 single crystals, Commun. Mater. **3**, 33 (2022).

[45] F. F. Balakirev, T. Kong, M. Jaime, R. D. McDonald, C. H. Mielke, A. Gurevich, P. C. Canfield, and S. L. Bud'ko, Anisotropy reversal of the upper critical field at low temperatures and spin-locked superconductivity in $K_2Cr_3As_3$, Phys. Rev. B **91**, 220505(R) (2015).

[46] N. Azari, M. Yakovlev, N. Rye, S. R. Dunsiger, S. Sundar, M. M. Bordelon, S. M. Thomas, J. D. Thompson, P. F. S. Rosa, and J. E. Sonier, Absence of spontaneous magnetic fields due to time-reversal symmetry breaking in bulk superconducting UTe_2, Phys. Rev. Lett. **131**, 226504 (2023).

[47] O. Tougait, M. Potel, and H. Noël, Crystal structure and magnetic properties of the binary triuranium pentatelluride U_2Te_5, J. Solid State Chem. **139**, 356 (1998).

[48] D. Li, A. Nakamura, F. Honda, Y. J. Sato, Y. Homma, Y. Shimizu, J. Ishizuka, Y. Yanase, G. Knebel, J. Flouquet *et al.*, Magnetic properties under pressure in novel spin-triplet superconductor UTe_2, J. Phys. Soc. Jpn. **90**, 073703 (2021).

[49] L. Onsager, Interpretation of the de Haas-van Alphen effect, Philos. Mag. **43**, 1006 (1952).

[50] R. B. Dingle, Some magnetic properties of metals II. The influence of collisions on the magnetic behaviour of large systems, Proc. R. Soc. A **211**, 517 (1952).

[51] T. I. Weinberger, Z. Wu, A. J. Hickey, D. E. Graf, G. Li, P. Wang, R. Zhou, A. Cabala, J. Pu, V. Sechovsky, M. Valiska, G. G. Lonzarich, F. M. Grosche, and A. G. Eaton, Pressure-enhanced f-electron orbital weighting in UTe_2 mapped by quantum interferometry, arXiv:2403.03946.

[52] C. T. Van Degrift, Tunnel diode oscillator for 0.001 ppm measurements at low temperatures, Rev. Sci. Instrum. **46**, 599 (2008).

[53] M. M. Altarawneh, C. H. Mielke, and J. S. Brooks, Proximity detector circuits: An alternative to tunnel diode oscillators for contactless measurements in pulsed magnetic field environments, Rev. Sci. Instrum. **80**, 066104 (2009).

[54] S. Ghannadzadeh, M. Coak, I. Franke, P. Goddard, J. Singleton, and J. L. Manson, Measurement of magnetic susceptibility in pulsed magnetic fields using a proximity detector oscillator, Rev. Sci. Instrum. **82**, 113902 (2011).

[55] The datasets supporting the findings of this Letter are available from the University of Cambridge Apollo Repository [10.17863/CAM.108558].

[56] Note that the calculation of $\mathcal{A}_{\lambda,\lambda'}$ is dependent on both the number and the direction of the trajectories included in λ and λ'.

[57] Each of $\mathcal{A}_\lambda = \{\mathcal{A}_\alpha, \mathcal{A}_\beta, \mathcal{A}_\gamma, \mathcal{A}_\delta\}$ have two distinct QI paths corresponding to them, each requiring only 4 instances of MB, which we label as $\lambda_{1,2}$.

[58] L. M. Falicov and H. Stachowiak, Theory of the de Haas-van Alphen effect in a system of coupled orbits. Application to magnesium, Phys. Rev. **147**, 505 (1966).

[59] I. M. Lifshitz and A. M. Kosevich, On the theory of the de Haas–van Alphen effect for particles with an arbitrary dispersion law, Dokl. Akad. Nauk SSSR **96**, 963 (1954).

[60] L. Miao, S. Liu, Y. Xu, E. C. Kotta, C.-J. Kang, S. Ran, J. Paglione, G. Kotliar, N. P. Butch, J. D. Denlinger, and L. A. Wray, Low energy band structure and symmetries of UTe_2 from angle-resolved photoemission spectroscopy, Phys. Rev. Lett. **124**, 076401 (2020).

[61] J. Ishizuka and Y. Yanase, Periodic Anderson model for magnetism and superconductivity in UTe_2, Phys. Rev. B **103**, 094504 (2021).

[62] D. Shaffer and D. V. Chichinadze, Chiral superconductivity in UTe_2 via emergent C_4 symmetry and spin-orbit coupling, Phys. Rev. B **106**, 014502 (2022).

[63] C. Broyles, Z. Rehfuss, H. Siddiquee, J. A. Zhu, K. Zheng, M. Nikolo, D. Graf, J. Singleton, and S. Ran, Revealing a 3D Fermi surface pocket and electron-hole tunneling in UTe_2 with quantum oscillations, Phys. Rev. Lett. **131**, 036501 (2023).

[64] H. C. Choi, S. H. Lee, and B.-J. Yang, Correlated normal state fermiology and topological superconductivity in UTe_2, arXiv:2206.04876.

[65] M. Sato and Y. Ando, Topological superconductors: A review, Rep. Prog. Phys. **80**, 076501 (2017).

[66] A similar effect, albeit less pronounced, may also be relevant for the Te p-band.

[67] http://mgml.eu.